Quantum Dot–Fluorescent Protein FRET Probes for Sensing Intracellular pH

Allison M. Dennis,[†,§] Won Jong Rhee,[‡] David Sotto,[†] Steven N. Dublin,[†,∥] and Gang Bao[†,*]

[†]Department of Biomedical Engineering, Georgia Institute of Technology and Emory University, 313 Ferst Drive, Atlanta, Georgia 30332, United States and [‡]Division of Bioengineering, University of Incheon, Incheon 406-772, Republic of Korea. [§]Present address: Centers for Integrated Nanotechnology, Los Alamos National Laboratory, Los Alamos, New Mexico 87545. [∥]Present address: QIAGEN Hamburg GmbH, Koenigstrasse 4a, 22767 Hamburg, Germany.

ABSTRACT

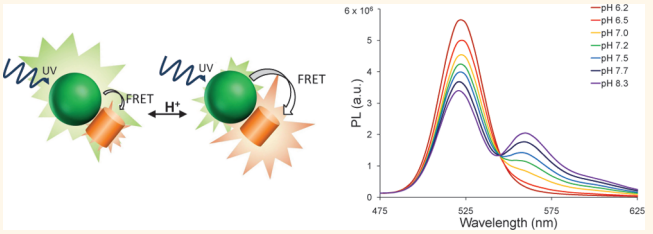

Intracellular pH (pH_i) plays a critical role in the physiological and pathophysiological processes of cells, and fluorescence imaging using pH-sensitive indicators provides a powerful tool to assess the pH_i of intact cells and subcellular compartments. Here we describe a nanoparticle-based ratiometric pH sensor, comprising a bright and photostable semiconductor quantum dot (QD) and pH-sensitive fluorescent proteins (FPs), exhibiting dramatically improved sensitivity and photostability compared to BCECF, the most widely used fluorescent dye for pH imaging. We found that Förster resonance energy transfer between the QD and multiple FPs modulates the FP/QD emission ratio, exhibiting a >12-fold change between pH 6 and 8. The modularity of the probe enables customization to specific biological applications through genetic engineering of the FPs, as illustrated by the altered pH range of the probe through mutagenesis of the fluorescent protein. The QD-FP probes facilitate visualization of the acidification of endosomes in living cells following polyarginine-mediated uptake. These probes have the potential to enjoy a wide range of intracellular pH imaging applications that may not be feasible with fluorescent proteins or organic fluorophores alone.

KEYWORDS: quantum dot · GFP-like fluorescent protein · FRET · pH sensing · intracellular sensing

Intracellular pH (pH_i) plays a critical role in the function of the cell, and its regulation is essential for most cellular processes, including cell volume regulation, vesicle trafficking, cellular metabolism, cell membrane polarity, cellular signaling, and cell activation, growth, and proliferation.[1,2] Cellular dysfunction is often associated with abnormal pH values in organelles, and low intracompartmental pH values can denature proteins or activate enzymes.[3] Abnormal pH_i can also affect human physiology such as the nervous system and pathophysiology including cancer[4] and Alzheimer's disease.[5] Monitoring pH changes inside living cells, therefore, is important for studying cellular functions and gaining a better understanding of physiological and pathological processes.

Intracellular pH can be measured with a variety of techniques, including the use of H^+ permeable microelectrodes, nuclear magnetic resonance (NMR), absorbance spectroscopy, and fluorescence imaging and spectroscopy.[2,6,7] Fluorescence spectroscopy using pH-sensitive indicators provides a powerful tool to assess the pH_i of intact cells and subcellular regions, which has several technical and practical advantages over other methods, including high sensitivity and excellent spatial and temporal resolution.[3] In particular, ratiometric measurements, *i.e.*, ratios obtained from simultaneous (or near simultaneous) fluorescence measurements at two (or more) excitation or emission wavelengths of the pH-sensitive probe, can eliminate the influence of variations in the local probe concentration, temperature, and optical path length.[8] High spatial resolution of pH_i indicators is critically important, since pH_i may vary significantly between subcellular compartments, including the cytosol, mitochondria, endoplasmic reticulum, endosome, lysosome, and nucleus.

While fluorescent indicators based on small organic dyes have been used to study the intracellular environment for some time, severe limitations based on the rapid photobleaching of these dyes disallow the tracking of cellular processes, and how they relate to pH, over time. Fluorescent indicators with higher sensitivity, improved signal-to-noise ratios, and better photostability could enable studies into subtle changes in the cytosolic pH with changes in the environment, cell health, or cell type. In addition, the ability to track pH temporally and spatially in a living cell could be utilized for visualizing the endosomal release of nanoparticle drug carriers, thus providing new insights into nanoparticle-based

* Address correspondence to gang.bao@bme.gatech.edu.

Received for review October 4, 2011 and accepted March 24, 2012.

Published online March 24, 2012
10.1021/nn2038077

targeted drug delivery approaches.[9,10] This information is crucial since endosomal release of drug carriers is necessary to enhance the efficacy of the drug being administered.

Our nanoparticle-based ratiometric pH sensor comprises a bright and photostable semiconductor quantum dot (QD) and pH-sensitive fluorescent proteins (FPs). The QD donor and pH-sensitive FP acceptors constitute a unique Förster resonance energy transfer (FRET) pair wherein the environmental sensitivity of the acceptor fluorophore modulates the emission intensity of the donor. QDs are particularly useful FRET donors due to their exceptional brightness, high quantum yields and photostability, the capacity to bind multiple acceptor molecules, and their broad excitation spectra and narrow, tunable emission spectra.[11,12] FPs are versatile FRET acceptors, as the polypeptide sequence can be genetically modified to include structural and functional elements necessary for protein purification, signal transduction, and probe assembly, as well as intracellular delivery and localization. FRET pairs comprising GFP-like FPs and QDs exhibit high energy transfer efficiencies and enable ratiometric measurements, resulting in heightened sensitivity by eliciting opposing changes in fluorescence emission at two wavelengths, while maintaining an internal control at an isosbestic point.[13−15]

RESULTS AND DISCUSSION

Probe Construction and Titration. We developed and characterized two QD-FP FRET-based pH sensors consisting of carboxyl-functionalized QDs conjugated to multiple copies of either mOrange, a bright, monomeric protein exhibiting pH sensitivity,[16] or its homologue mOrange M163K, a mutant with shifted pK_a (the pH at which the measured property is half its maximum) and improved photostability.[17] Both the excitation and emission spectra of the FPs vary with pH due to the pH dependence of their molar extinction coefficients (Supplementary Figures S1, S2, and S3). As a result, the spectral overlap of the FRET pair and thus the efficiency of energy transfer directly correlate to the pH of the environment and exhibit maximum sensitivity near the pK_a of the acceptor FP. In contrast to an acceptor whose quantum yield is environmentally sensitive, the pH-specific modulation of the acceptor absorbance results in a probe where both the donor quenching and the sensitized acceptor emission are affected by changes in pH. This synergistic effect increases the pH-dependent change in the ratio of acceptor and donor emission intensities, thus improving probe sensitivity. With pK_a values of 6.9 and 7.9, respectively, mOrange and mOrange M163K are appropriate acceptors for sensitive detection in or near the physiological pH range. FPs were conjugated to QDs *via* standard carbodiimide chemistry,[18] with absorbance spectroscopy indicating an average of 15.7 and 16.5 proteins per QD for the mOrange and mOrange M163K probes, respectively (Figure 1b). This conjugation method covalently links primary amines in the proteins to carboxylic acids on the surface of the QDs, ensuring that the probe assembly is not susceptible to changes in pH. This method, however, does not give full control of the protein orientation on the surface of the QD. It is also possible to have protein aggregation or the attachment of FPs to other FPs already bound to the surface of a QD, leading to a variety of donor−acceptor distances, as discussed below. The presence of FPs on the QD surface as confirmed by the absorption spectra (Figure 1b), dynamic light scattering (DLS) measurements (Supplementary Figure S4), and the evidence that simply mixing QDs and FPs without conjugation does not induce FRET signal (Supplementary Figure S6b) demonstrates the successful conjugation of FPs to the QD surface, although the valence and orientation of FPs are unknown. Thus, the average numbers of FPs per QDs are in fact the maximum average number of proteins bound to each QD, not an exact estimate of donor−acceptor ratios of the conjugate.

At alkaline pH values, under QD excitation at 400 nm, the QD−mOrange probe demonstrates strong energy transfer, as indicated by the sensitized emission of mOrange at 560 nm. With reduction in pH, the mOrange emission peak intensity decreases and the QD emission peak intensity increases as changes in the mOrange absorbance reversibly modulate the emission from the pH-insensitive QD (Figure 1, Supplementary Figures S5 and S6a). The clear isosbestic point at 540 nm could be used to calibrate differences in conditions between multiple samples. The ratio of the acceptor (560 nm) to donor (520 nm) emission peaks (F_A/F_D) increased by >12-fold between pH 6 and 8 and ~20-fold over the range of pH values tested (5−10), with excellent repeatability (Figure 1e, $n = 3$). The sigmoidal fit to the data indicates a pK_a of 7.0 for the QD−mOrange probe. No sensitized emission of mOrange was detectable below pH 6, and the FRET efficiency was greater than 0.55 for pH values above 8. Titration of QD−mOrange M163K probes yielded similar trends, with ~16-fold change in F_A/F_D over pH 5−10 and a pK_a of 7.4. In contrast, titration of the fluorophore BCECF yields a pK_a of 6.9 and a <5-fold change in signal (Figure 1f and Supplementary Figure S7).

FRET Analysis. Quantitative FRET analysis demonstrated that overlap integrals and Förster distances vary with pH in accordance with the pH-dependent change in the FP optical properties (Figure 2). The pH-dependent FRET efficiencies were calculated by comparing the QD emission intensity at a specific pH to the QD emission intensity at the most acidic measurement in a titration. Under acidic conditions, the FPs are "dead" in that at the emission wavelength of the QDs they do not exhibit the absorption properties necessary for energy transfer. By using this QD emission

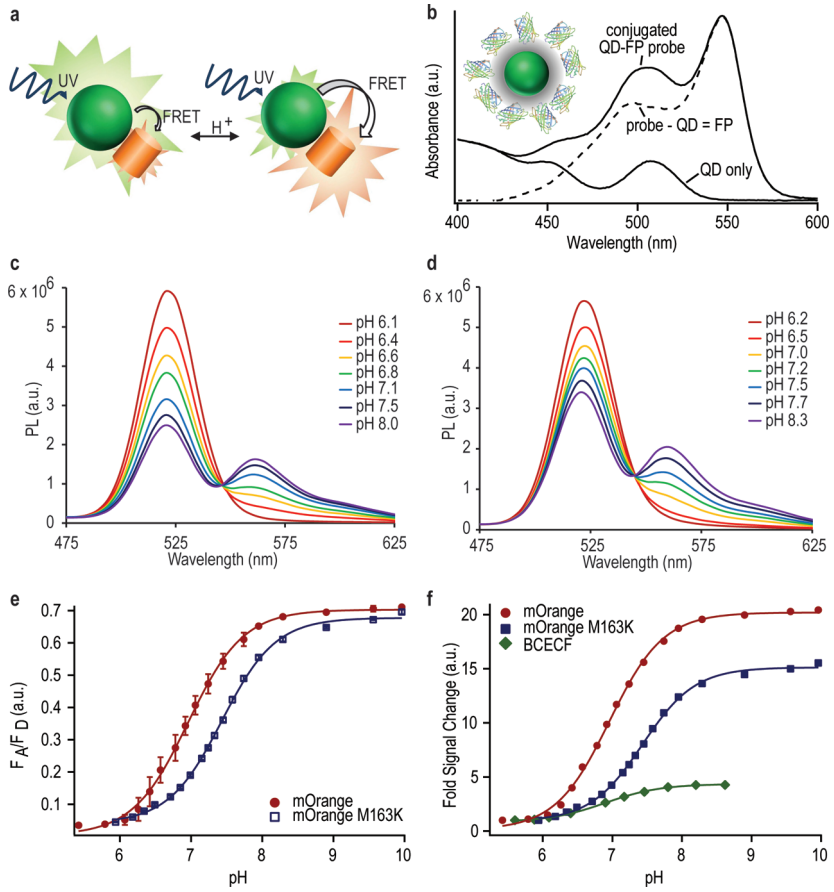

Figure 1. QD-FP FRET-based pH sensor. (a) Schematic demonstration of the pH-dependent energy transfer between the quantum dot and fluorescent protein. In an acidic environment, energy transfer to the FP FRET acceptor is minimal, yielding a high QD signal; at neutral or basic pH, energy transfer is more efficient, producing an enhanced FRET signal. (b) Absorbance spectroscopy indicates multiple proteins bound to each QD, as depicted in the inset. (c and d) Titration of QD-FP probes containing the FP acceptors mOrange and mOrange M163K, respectively, showing increased energy transfer at alkaline pHs with clear isosbestic points. Representative spectra of one of three independent titrations are shown. (e) The ratio of acceptor emission to donor emission increases with increasing pH for both probes. Data points are means ± standard deviations for three independent titrations. (f) The changes in the nanoprobe acceptor to donor ratios are compared to the ratiometric signal change for the pH-sensitive fluorophore BCECF. One representative titration is shown.

value, rather than the emission of QDs in the absence of the FPs, we are isolating the pH-dependent energy transfer from any external factors, such as differences in concentration and instrument settings, changes to the QD during the conjugation procedure, or effects due to the presence of the protein.

We estimated the average donor–acceptor distance for this system as described in the Methods section and found that the donor–acceptor distance calculated is reasonably constant for both probes, as demonstrated in Figure 2d. However, the estimated donor–acceptor distances increased slightly with pH values, most likely an artifact due to the assumptions we made in the distance calculations. Specifically, the number of acceptors per donor we used in the analysis is the maximum number possible after FP conjugation, rather than a precise value (as discussed above). Further, our conjugation method resulted in a variety of FP positions and orientations relative to the QD surface, suggesting that the estimated donor–acceptor distance is an average of a significant range of distances. Nevertheless, the roughly constant donor–acceptor distance calculated for mOrange–QD probes supports the hypothesis that, in our QD–FP pH sensors, changes in the FP optical properties affect the FRET efficiency, rather than the donor–acceptor distance. This is in sharp contrast to distance-based FRET signal transduction, in which the FRET efficiencies increase dramatically as the donor–acceptor distance is shortened.[18,19]

Photobleaching. Many common pH-sensitive fluorophores are notorious for their lack of photostability.[19] Although mOrange suffers from increased photolability compared to other GFP-like fluorescent proteins,[16] integration of the FP into the FRET probe improved its useful lifetime dramatically, since QD excitation with ultraviolet radiation does not directly excite the FP chromophore. When excited directly with a fluorescence microscope, the mOrange signal diminished >60% in 15 s and 80% under 60 s of continuous illumination. However, it takes >28 min to reduce the sensitized emission of mOrange by 80% under continuous

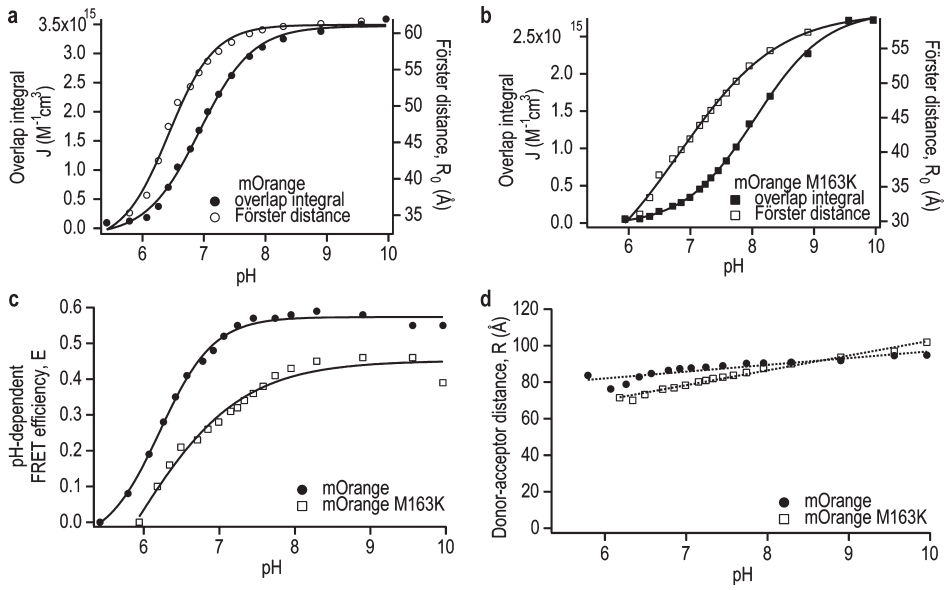

Figure 2. FRET analysis. (a and b) Calculated overlap integral, *J*, and Förster distance, R_0, as a function of pH for QD-FP FRET probes containing mOrange and mOrange M163K, respectively. (c) FRET efficiency for both probes over the relevant pH range. (d) Donor−acceptor distance *versus* pH for the probes containing mOrange and mOrange M163K. Data shown in (c) and (d) are representative of one of three independent titrations.

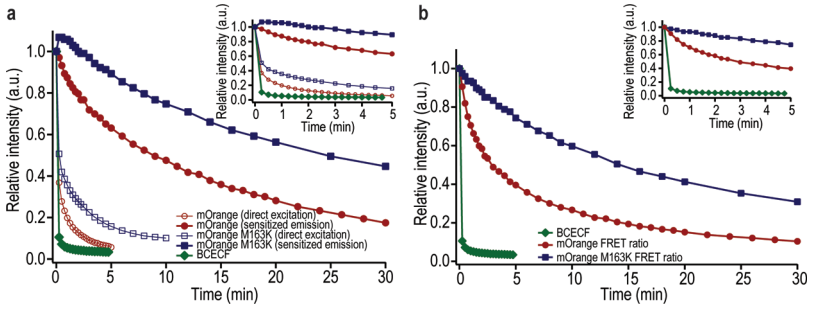

Figure 3. Photostability. The photostability of the fluorescent proteins and FRET-based pH sensors is compared to that of BCECF, a pH-sensitive fluorophore, during continuous illumination in a fluorescence microscope. (a) Relative intensity of the fluorescent protein emission in the FRET probes when excited directly or through the FRET mechanism, resulting in sensitized emission. (b) Acceptor/donor emission ratio as a function of time for the QD−mOrange and QD−mOrange M163K probes with continuous excitation of the QD donor. Relative intensity of BCECF emissions with continuous excitation is also shown for comparison. The differences at short time scales are highlighted in the insets of (a) and (b). Shown here are representative results of one of three independent experiments.

excitation of the QD. In contrast, emission from the pH-sensitive fluorophore BCECF decreased by 90% after just 15 s of continuous illumination (Figure 3a). The M163K mutation improves the photostability of mOrange, and the QD−mOrange M163K FRET probe likewise exhibited a considerably increased useful lifetime through the FRET mechanism. Consequently, the QD−FP probes containing mOrange and mOrange M163K exhibited rather robust F_D/F_A values under the harsh conditions of continuous illumination (Figure 3b). The significantly improved photostability compared to BCECF enables a wide range of imaging applications, including the use of time-lapse imaging for real-time tracking of the probes.

Intracellular Imaging. Our QD−FP pH probes clearly exceed the minimum criteria for effective intracellular FRET probes, defined as a FRET efficiency exceeding 0.1 and a greater than 30% change in the acceptor to donor emission ratio.[20] Importantly, our probes are most responsive around physiological pH values, and the excitation and emission wavelengths of the donor (QD) and acceptor (FP) correspond to common filter sets, enabling measurements with existing detection modalities, such as fluorescence microscopes and flow cytometers.

To demonstrate the ability to image intracellular pH changes temporally and spatially, we performed live-cell fluorescence microscopy with a modified QD−mOrange probe containing a C-terminal polyarginine sequence for cellular delivery. The inclusion of this peptide facilitates the endosomal uptake of QD−FP constructs.[21] We incubated cultured HeLa cells with the nanoprobe for an hour, rinsed away unbound probes, and imaged over several time points using

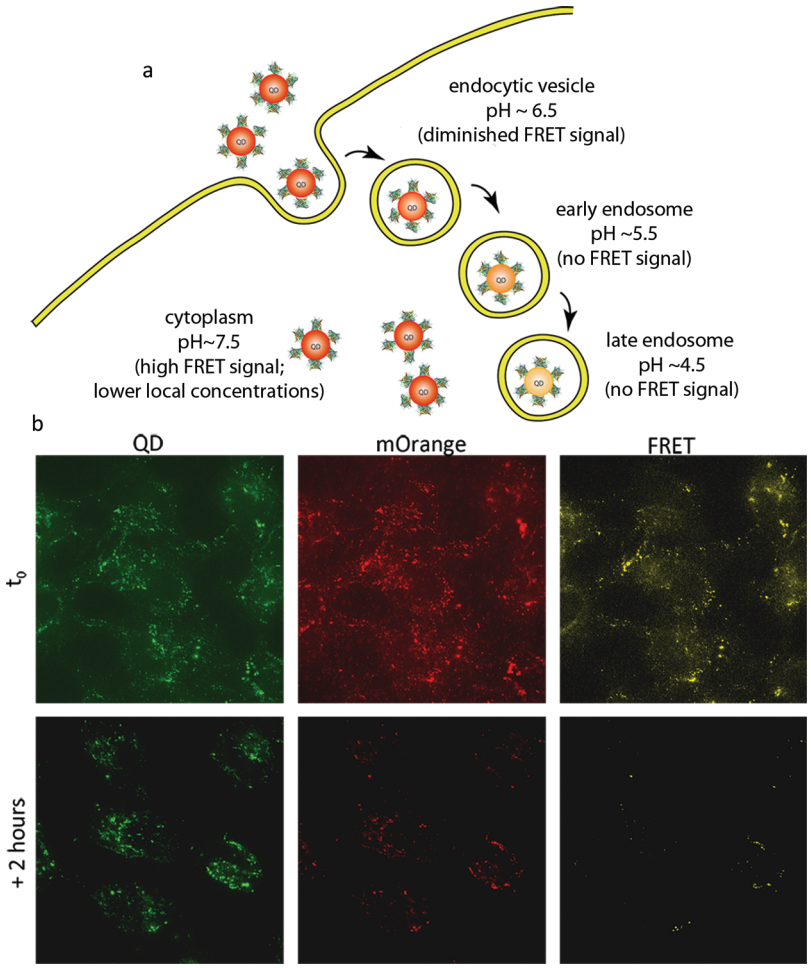

Figure 4. Cellular imaging of QD−mOrange pH sensor. (a) Schematic of probe color changes during progression through the endocytic pathway. FRET efficiency is high in the neutral pH of the extracellular environment and early endosome. FRET efficiency decreases as the endosome matures and the endosomal pH drops, resulting in diminished emission from mOrange and recovery of some QD signal. Any probe that escapes the endosome regains its elevated FRET efficiency in the pH neutral cytoplasm. (b) Fluorescence microscopy images immediately after delivery of the probe and two hours postdelivery. The QD images (left) demonstrate consolidation of the probe in the endosomes over time; images of the direct excitation of mOrange (center) and FRET emission (right) indicate a clear decrease in the mOrange emission and the FRET efficiency of the probe with maturation of the endosome.

filter sets that selected for (1) the direct excitation and emission of the QD, (2) the direct excitation and emission of mOrange, and (3) the FRET signal, *i.e.*, excitation of the QD and emission of mOrange. We hypothesized that as the QD−FP probes progress from endocytotic vesicles to the early endosome to the late endosome, the drop in pH should induce changes in the probe signal, decreasing the mOrange and FRET signals (Figure 4a). This was indeed observed 2 h after probe delivery, as indicated by the much reduced mOrange signal (under direct excitation) and FRET signal (mOrange emission under QD excitation) (Figure 4b), consistent with the results shown in Figure 1. Although the change in QD signal after 2 h is not as apparent as that of FP, there was an estimated 1.5−2-fold increase in QD signal (the exact fold increase of QD signal varies from cell to cell). Note that all the fluorescence images in Figure 4 were taken under exactly the same optical conditions, and the same brightness and contrast was applied to the images by the microscope automatically. The difference in contrasts in the top and bottom panels of Figure 4 could be due to photobleaching of autofluorescent biomolecules present in the 10% fetal bovine serum (FBS) in the cell media; however the exact reason remains unknown. This issue will be addressed systematically in subsequent cellular imaging studies.

As a negative control, HeLa cells were treated with bafilomycin A and nocodazole, which inhibit the maturation of the endosome.[22] We found that inhibition of endosomal acidification eliminated changes in the FRET signal from the pH nanosensor 2 h after probe delivery (Figure 5a), suggesting that changes seen in Figure 4b were due to pH changes. To rule out the possibility that the FP signal changes were due to proteolytic degradation of the fluorescent protein, we delivered a polyarginine-tagged QD−FP probe containing the relatively pH-insensitive FP mCherry into HeLa cells for imaging (Figure 5b, Supplementary

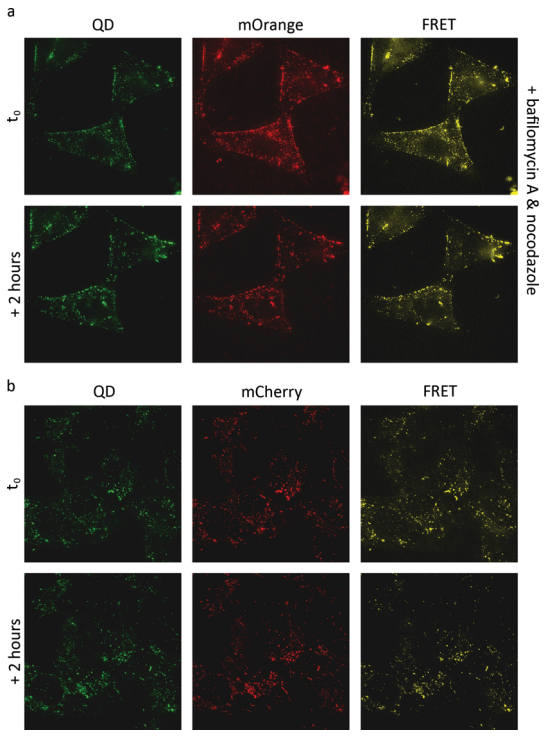

Figure 5. Control studies for cellular imaging. (a) Fluorescence microscopy images immediately after delivery of the probe and two hours after delivery into cells pretreated with bafilomycin A and nocodazole, drugs that arrest the endosomal progression. The QD images (left) demonstrate consolidation of the probe in the endosomes over time; images of the direct excitation of mOrange (center) and FRET emission (right) are similar at both time points, indicating an unchanged pH due to the drug treatment. (b) Fluorescence microscopy images immediately after delivery and two hours postdelivery of an mCherry-based QD–FP probe that shows less pH sensitivity than the mOrange-based probes. The persistence of the mCherry and FRET signals after two hours indicates that the probe, including the fluorescent protein, survives endosomal maturation intact.

Figure S7). The persistence of the mCherry and FRET signals from the nanoprobe at the later time point indicates that the barrel structure of GFP-like FPs does endure the endosomal environment, consistent with the literature.[23] For intracellular pH sensing experiments, which typically require less than two hours of fluorescence microscopy, the potential cytotoxicity of the QD–FP probes is not a concern (Supplementary Figure S8).

Although the unique optical properties of QDs lead to improved FRET-based biosensor designs,[11,12] to date only limited success has been demonstrated for intracellular applications of QD-based biosensors,[24] including the approaches utilizing the inherent sensitivity of certain QDs to the intracellular environment (such as ion concentration or pH)[25] or an energy transfer mechanism.[26,27] The probes reported thus far are not ratiometric and, therefore, lack an internal control for extrinsic factors such as changes in the local probe concentration or optical path length. Other limited examples of QD-based pH sensing in solution using FRET lack sensitivity in the physiological pH range, thus may not be suitable for intracellular pH sensing.[28,29] Other sensor designs that utilize both nanoparticle platforms and pH-sensitive fluorophores have demonstrated an impressive pH range[30–33] and applicability in the intracellular milieu,[33] but are either less sensitive (as determined by examining the fold signal change as in Figure 1f) than our probe[30–32] or do not report sensitivity in a way that enables comparison to the probe described here.[33] None of these studies address the photostability issue of the probes. The strategy of using multiple fluorophores with complementary pK_a values in tandem to extend the pH sensor's dynamic range works very well for dye-loaded polymeric nanoparticles.[33] A similar extension of the dynamic range of the probes described here may be possible by employing multiple FP acceptors with various pK_a values.

A primary advantage of this probe design is its inherent modularity. The customization of FP properties through genetic engineering enables the development of probes with an optimal range of sensitivities and optical properties. For example, the useful lifetime of QD–FP probes could be further improved by using GFP-like fluorescent proteins with photobleaching half-lives longer than those of mOrange and mOrange M163K. Other protein variants maintain their optical properties up to 20 times longer than mOrange.[17] Furthermore, the engineering of the FP sensitivities could result in a range of analytes that could be monitored using this nanoprobe approach. FPs with sensitivities to chloride and copper have already been identified,[34,35] and screening methods could be used to develop FPs for use in other environmental sensors. Conveniently, the methods to modify these FPs are readily available in any molecular biology lab and do not rely on proprietary, expensive, or technically arduous syntheses. Thus, a toolbox of sensitive, photostable biosensors could be developed using long-lived FPs selected for their environmental sensitivities and appropriately color-matched QD donors.

CONCLUSIONS

In summary, we have demonstrated the unique features of the novel QD–FP probes for FRET-based sensing of pH_i, including high sensitivity and wide dynamic range, ratiometric measurements for internal calibration, dramatic reduction of photobleaching, and the ability to tailor the probe design for different pH ranges. These probes are well suited to a wide range of intracellular pH-dependent imaging applications that are not feasible with fluorescent proteins or organic fluorophores alone. For example, one could use QD–mOrange probes for tracking the endosomal release of nanocarriers for drug/gene delivery and mOrange M163K probes for pH mapping of the cytosol. We envision that, by tailoring the FP to the specific application,

this type of QD–FP FRET probe could be used for sensitive and multiplexed monitoring of environmental analytes such as pH and metal ion concentration in both the intracellular and extracellular environment.

MATERIALS AND METHODS

FRET Probe Preparation. The QD–FP probes were assembled by incubating a 1 μM solution of 525 nm emitting Qdot ITK carboxyl quantum dots (Life Technologies, formerly Invitrogen, Carlsbad, CA, USA) with a 40-fold excess of the appropriate protein and a 1500-fold excess of 1-ethyl-3-(3-dimethylaminopropyl)carbodiimide (EDC; Pierce, Rockford, IL, USA) overnight at 4 °C with gentle shaking. Byproducts, unreacted EDC, and excess protein were removed using a centrifugal filtration device with a 100 kDa molecular weight cutoff (Microcon Ultracel YM-100, Millipore, Bedford, MA, USA) at 1000 rcf. Dynamic light scattering measurements indicate that the average hydrodynamic diameter of the QDs is 14.5 ± 1.5 nm and that for the QD–FP probes is 25.1 ± 2.3 nm (Supplemental Figure S4).

FRET Measurements and Analysis. The spectral characteristics of the FRET probe were measured over a range of pHs by diluting 15 pmol of the probe in 500 μL of 20 mM phosphate-buffered saline + 1% (w/v) bovine serum albumin, pH 10.0, and titrating with 1 N HCl. Fluorescence emission spectra were measured with a Horiba Jobin Yvon Fluorolog-3 spectrofluorimeter with excitation at 400 nm, 1 nm excitation bandwidth, 3 nm emission bandwidth, and 5 nm stepsize. Following titration with HCl, a bolus of 1 N NaOH was added to demonstrate the reversibility of the pH probe. Controls included titration of unconjugated QDs and fluorescence spectroscopy of a mixture FPs and QDs (unconjugated) to ensure the pH stability of the QDs and the lack of direct excitation of the mOrange under the experimental conditions, respectively (Supplemental Figure S3).

The QD emission spectrum and the protein excitation spectra over the range of pHs were used to calculate the spectral overlap integral:

$$J = \int F_D(\lambda)\, \varepsilon_A(\lambda)\lambda^4\, d\lambda$$

where F_D is the emission spectrum of the QD donor, ε_A is the molar extinction coefficient of the protein acceptor at that pH, and λ is the wavelength in nanometers.[36] The overlap integral is used to calculate the Förster distance, R_0, *i.e.*, the distance between the donor and acceptor at which the FRET efficiency is 50%, using the equation

$$R_0^6 = (8.785 \times 10^{-5})\kappa^2 Q_D J \eta^{-4}$$

where κ^2 is the dipole orientation factor, assumed to be 2/3, QD is the quantum yield of the donor, and η is the refractive index of the medium.[36]

The FRET efficiencies (E) over the range of pH values were calculated using the equation

$$E = 1 - \frac{F_{DA}}{F'_{DA}}$$

where F_{DA} is the QD emission at 520 nm of a conjugated probe at the given pH, and F'_{DA} is the QD emission from that same probe at the most acidic pH measured, *i.e.*, where the energy transfer to the protein is negligible. Using this method, the FRET efficiency at the most acidic point measured is inherently defined as zero. In calculating the average donor–acceptor distance (R) at each point using the equation below, the average number of acceptors per donor, n, as determined using absorbance spectroscopy (Supplementary Figure S3), was taken into account, but the Poisson distribution of the actual number of acceptors per donor was neglected because it has little effect on constructs containing greater than five acceptors per donor:[37]

$$E = \frac{nR_0^6}{nR_0^6 + R^6}$$

Photobleaching. Samples were prepared for photobleaching experiments by mixing a 0.5 μM solution of conjugated probe with four times the volume of water-extracted mineral oil to create bubbles of probe within the oil. The mixture was sealed between a glass slide and coverslip and mounted on a DeltaVision fluorescence microscope (Applied Precision, LLC, Issaquah, WA, USA). mOrange and mOrange M163K were excited directly using a TRITC filter set (555/28 excitation and 617/63 emission). The sensitized emission of the mOranges resulting from FRET was examined by exciting the sample with a DAPI excitation filter (360/40) while monitoring the fluorescent protein emission through the TRITC emission filter, while a combination of the DAPI excitation and GFP emission filters (525/50) was used to image the QD signal. The intensity value for each time point was noted as an average of 361 pixels. The background signal was subtracted from this value prior to normalizing the data to see the rate of photobleaching. The same procedure was followed to measure the photobleaching of 2′,7′-bis(2-carboxyethyl)-5-(and-6)-carboxyfluorescein (BCECF; Life Technologies) using the FITC excitation (490/20) and emission (526/38) filter set.

Intracellular Imaging. HeLa cells were cultured in 8-well Lab-Tek II chambered cover glasses (Nalgene Nunc International, NY, USA). QD–mOrange–Arg9 or QD–mCherry–Arg9 probes were delivered by incubation with the cells in Opti-MEM at a concentration of 50 nM for 1 h at 37 °C. The cells were then rinsed three times before being covered with Opti-MEM containing 10% FBS. After delivery, the same cells were monitored for 2 h with the same optical conditions for each filter set (QD: DAPI excitation, GFP emission; FP: TRITC excitation and emission; FRET: DAPI excitation, TRITC emission). The cells were maintained in a controlled environment at 37 °C and 5% CO_2 throughout imaging. To block the endocytic pathway, cells were preincubated with 400 nM bafilomycin A and 20 μM nocodazole in Opti-MEM for 30 min before delivering the QD–mOrange probes. QD–mOrange–Arg9 probes were then added to the medium at a final concentration of 50 nM for delivery.

Live-cell fluorescence imaging was performed using a DeltaVision Deconvolution microscope equipped with an Olympus 60×, Plan Apo N lens, numerical aperture 1.42, and a CoolSNAP_HQ2/ICX285 camera. Images were collected at 0.2 μm Z-intervals.

Conflict of Interest: The authors declare no competing financial interest.

Acknowledgment. This work was supported by the National Institutes of Health as an NHLBI Program of Excellence in Nanotechnology Award (HHSN268201000043C to G.B.) and as an NIH Nanomedicine Development Center Award (PN2EY018244 to GB) and by the National Science Foundation as a Science and Technology Center Grant (CBET- 0939511).

Supporting Information Available: Details of the protein preparation and characterization; probe titration; and BCECF and mCherry characterization. This material is available free of charge via the Internet at http://pubs.acs.org.

REFERENCES AND NOTES

1. Busa, W. B.; Nuccitelli, R. Metabolic Regulation via Intracellular pH. *Am. J. Physiol.* **1984**, *246*, R409–R438.
2. Loiselle, F. B.; Casey, J. R. Measurement of Intracellular pH. *Methods Mol. Biol.* **2003**, *227*, 259–280.
3. Han, J.; Burgess, K. Fluorescent Indicators for Intracellular pH. *Chem. Rev.* **2010**, *110*, 2709–2728.
4. Izumi, H.; Torigoe, T.; Ishiguchi, H.; Uramoto, H.; Yoshida, Y.; Tanabe, M.; Ise, T.; Murakami, T.; Yoshida, T.; Nomoto, M.; Kohno, K. Cellular pH Regulators: Potentially Promising Molecular Targets for Cancer Chemotherapy. *Cancer Treatment Rev.* **2003**, *29*, 541–549.

5. Davies, T. A.; Fine, R. E.; Johnson, R. J.; Levesque, C. A.; Rathbun, W. H.; Seetoo, K. F.; Smith, S. J.; Strohmeier, G.; Volicer, L.; Delva, L.; Simons, E. R. Non-Age Related Differences in Thrombin Responses by Platelets from Male Patients with Advanced Alzheimer's Disease. *Biochem. Biophys. Res. Commun.* **1993**, *194*, 537–543.
6. Wray, S. Smooth Muscle Intracellular pH: Measurement, Regulation, and Function. *Am. J. Physiol.* **1988**, C213–C225.
7. Kotyk, A. S.; Slavík, J. *Intracellular pH and Its Measurement*. CRC: Boca Raton, FL, 1989.
8. Grant, R. L.; Acosta, D. Ratiometric Measurement of Intracellular pH of Cultured Cells with BCECF in a Fluorescence Multi-Well Plate Reader. *In Vitro Cell Dev. Biol. Anim.* **1997**, *33*, 256–260.
9. Panyam, J.; Zhou, W. Z.; Prabha, S.; Sahoo, S. K.; Labhasetwar, V. Rapid Endo-lysosomal Escape of Poly(DL-lactide-co-glycolide) Nanoparticles: Implications for Drug and Gene Delivery. *FASEB J.* **2002**, *16*, 1217–1226.
10. Duan, H.; Nie, S. Cell-Penetrating Quantum Dots Based on Multivalent and Endosome-Disrupting Surface Coatings. *J. Am. Chem. Soc.* **2007**, *129*, 3333–3338.
11. Medintz, I. L.; Mattoussi, H. Quantum Dot-Based Resonance Energy Transfer and its Growing Application in Biology. *Phys. Chem. Chem. Phys.* **2009**, *11*, 17–45.
12. Algar, W. R.; Krull, U. J. Quantum Dots as Donors in Fluorescence Resonance Energy Transfer for the Bioanalysis of Nucleic Acids, Proteins, and Other Biological Molecules. *Anal. Bioanal. Chem.* **2008**, *391*, 1609–1618.
13. Dennis, A. M.; Bao, G. Quantum Dot-Fluorescent Protein Pairs As Novel Fluorescence Resonance Energy Transfer Probes. *Nano Lett.* **2008**, *8*, 1439–45.
14. Boeneman, K.; Mei, B. C.; Dennis, A. M.; Bao, G.; Deschamps, J. R.; Mattoussi, H.; Medintz, I. L. Sensing Caspase 3 Activity with Quantum Dot-Fluorescent Protein Assemblies. *J. Am. Chem. Soc.* **2009**, *131*, 3828–9.
15. Dennis, A. M.; Sotto, D. C.; Mei, B. C.; Medintz, I. L.; Mattoussi, H.; Bao, G. Surface Ligand Effects on Metal-Affinity Coordination to Quantum Dots: Implications for Nanoprobe Self-Assembly. *Bioconjugate Chem.* **2010**, *21*, 1160–1170.
16. Shaner, N. C.; Campbell, R. E.; Steinbach, P. A.; Giepmans, B. N.; Palmer, A. E.; Tsien, R. Y. Improved Monomeric Red, Orange and Yellow Fluorescent Proteins Derived from Discosoma sp. Red Fluorescent Protein. *Nat. Biotechnol.* **2004**, *22*, 1567–72.
17. Shaner, N. C.; Lin, M. Z.; McKeown, M. R.; Steinbach, P. A.; Hazelwood, K. L.; Davidson, M. W.; Tsien, R. Y. Improving the Photostability of Bright Monomeric Orange and Red Fluorescent Proteins. *Nat. Methods* **2008**, *5*, 545–551.
18. Hermanson, G. T. *Bioconjugate Techniques*, 2nd ed.; Academic Press: San Diego, CA, 2008.
19. Han, J. Y.; Burgess, K. Fluorescent Indicators for Intracellular pH. *Chem. Rev.* **2010**, *110*, 2709–2728.
20. Campbell, R. E. Fluorescent-Protein-Based Biosensors: Modulation of Energy Transfer as a Design Principle. *Anal. Chem.* **2009**, *81*, 5972–5979.
21. Medintz, I. L.; Pons, T.; Delehanty, J. B.; Susumu, K.; Brunel, F. M.; Dawson, P. E.; Mattoussi, H. Intracellular Delivery of Quantum Dot-Protein Cargos Mediated by Cell Penetrating Peptides. *Bioconjugate Chem.* **2008**, *19*, 1785–1795.
22. Bayer, N.; Schober, D.; Prchla, E.; Murphy, R. F.; Blaas, D.; Fuchs, R. Effect of Bafilomycin A1 and Nocodazole on Endocytic Transport in HeLa Cells: Implications for Viral Uncoating and Infection. *J. Virol.* **1998**, *72*, 9645–9655.
23. Katayama, H.; Yamamoto, A.; Mizushima, N.; Yoshimori, T.; Miyawaki, A. GFP-Like Proteins Stably Accumulate in Lysosomes. *Cell Struct. Funct.* **2008**, *33*, 1–12.
24. Li, Z.; Wang, Y. X.; Zhang, G. X.; Xu, W. B.; Han, Y. J. Chemiluminescence Resonance Energy Transfer in the Luminol-CdTe Quantum Dots Conjugates. *J. Lumin.* **2010**, *130*, 995–999.
25. Liu, Y. S.; Sun, Y. H.; Vernier, P. T.; Liang, C. H.; Chong, S. Y. C.; Gundersen, M. A. pH-Sensitive Photoluminescence of CdSe/ZnSe/ZnS Quantum Dots in Human Ovarian Cancer Cells. *J. Phys. Chem. C* **2007**, *111*, 2872–2878.
26. Medintz, I. L.; Stewart, M. H.; Trammell, S. A.; Susumu, K.; Delehanty, J. B.; Mei, B. C.; Melinger, J. S.; Blanco-Canosa, J. B.; Dawson, P. E.; Mattoussi, H. Quantum-Dot/Dopamine Bioconjugates Function as Redox Coupled Assemblies for in Vitro and Intracellular pH Sensing. *Nat. Mater.* **2010**, *9*, 676–684.
27. Tomasulo, M.; Yildiz, I.; Kaanumalle, S. L.; Raymo, F. M. pH-Sensitive Ligand for Luminescent Quantum Dots. *Langmuir* **2006**, *22*, 10284–10290.
28. Snee, P. T.; Somers, R. C.; Nair, G.; Zimmer, J. P.; Bawendi, M. G.; Nocera, D. G. A Ratiometric CdSe/ZnS Nanocrystal pH Sensor. *J. Am. Chem. Soc.* **2006**, *128*, 13320–13321.
29. Suzuki, M.; Husimi, Y.; Komatsu, H.; Suzuki, K.; Douglas, K. T. Quantum Dot FRET Biosensors that Respond to pH, to Proteolytic or Nucleolytic Cleavage, to DNA Synthesis, or to a Multiplexing Combination. *J. Am. Chem. Soc.* **2008**, *130*, 5720–5725.
30. Zhang, F.; Ali, Z.; Amin, F.; Feltz, A.; Oheim, M.; Parak, W. J. Ion and pH Sensing with Colloidal Nanoparticles: Influence of Surface Charge on Sensing and Colloidal Properties. *ChemPhysChem* **2010**, *11*, 730–735.
31. Chen, Y.; Thakar, R.; Snee, P. T. Imparting Nanoparticle Function with Size-Controlled Amphiphilic Polymers. *J. Am. Chem. Soc.* **2008**, *130*, 3744–3745.
32. Jin, T.; Sasaki, A.; Kinjo, M.; Miyazaki, J. A Quantum Dot-Based Ratiometric pH Sensor. *Chem. Commun.* **2010**, *46*, 2408–2410.
33. Benjaminsen, R. V.; Sun, H. H.; Henriksen, J. R.; Christensen, N. M.; Almdal, K.; Andresen, T. L. Evaluating Nanoparticle Sensor Design for Intracellular pH Measurements. *ACS Nano* **2011**, *5*, 5864–5873.
34. Markova, O.; Mukhtarov, M.; Real, E.; Jacob, Y.; Bregestovski, P. Genetically Encoded Chloride Indicator with Improved Sensitivity. *J. Neurosci. Methods* **2008**, *170*, 67–76.
35. Sumner, J. P.; Westerberg, N. M.; Stoddard, A. K.; Hurst, T. K.; Cramer, M.; Thompson, R. B.; Fierke, C. A.; Kopelman, R. DsRed as a Highly Sensitive, Selective, and Reversible Fluorescence-Based Biosensor for Both Cu^{+} and Cu^{2+} Ions. *Biosens. Bioelectron.* **2006**, *21*, 1302–1308.
36. Lakowicz, J. R. *Principles of Fluorescence Spectroscopy*, 3rd ed.; Springer: New York, 2006.
37. Pons, T.; Medintz, I. L.; Wang, X.; English, D. S.; Mattoussi, H. Solution-Phase Single Quantum Dot Fluorescence Resonance Energy Transfer. *J. Am. Chem. Soc.* **2006**, *128*, 15324–15331.